A Novel Approach to Model Linear and Nonlinear Dispersion

Michael Ammann[1], Stefan Schild[1], Nicolas Chavannes[2] and Niels Kuster[1]
[1] IT'IS Foundation for Research on Information Technologies in Society (IT'IS) - ETH Zurich, Switzerland
[2] Schmid & Partner Engineering AG (SPEAG), Zurich, Switzerland

INTRODUCTION

Nowadays, a big effort is made in the investigation of structures to control and manipulate electromagnetic waves. Among these structures are photonic crystals (PC), negative indexed metamaterials (NIM) and optical fibres which are difficult and expensive to manufacture in order to investigate their electromagnetic properties. The finite-difference time-domain (FDTD) method has proven to be a very efficient computational tool for simulating electromagnetic fields in arbitrarily complex structures. While it may be sufficient for many applications to simulate the photonic structures in the linear dispersive regime, a growing number of applications is exploiting nonlinear dispersion.

The FDTD method has one major drawback regarding its application to optics and photonics: The required spatial and temporal discretisation depend on the simulated wavelength. In optics, the simulated objects are much larger than the simulated wavelength resulting in extremely large grids requiring large computational resources. State-of-the-art FDTD software is hardware accelerated. To perform real world simulations, it is hence imperative that an efficient 3D-algorithm allows update splitting (polarisations can be updated seperately and contribute an additive constant to the standard FDTD update) in order to distribute the work load between hardware and software.

METHODOLOGY

A new FDTD algorithm capable of solving the full-vector Maxwell's equations in linear and nonlinear dispersive materials is proposed that allows parallelisation. At the core of the new approach lies a very efficient treatment of the Kerr-effect.

Consider Ampere's law

$$\begin{aligned}\nabla \wedge \mathbf{H} &= \frac{\partial \mathbf{D}}{\partial t} + \mathbf{j} \\ &= \epsilon_0\epsilon_\infty \frac{\partial \mathbf{E}}{\partial t} + \frac{\partial \mathbf{P_{tot}}}{\partial t} + \sigma \mathbf{E}\end{aligned} \tag{1.1}$$

assuming that Ohm's law j = σE is valid. For a medium with L Lorentz-poles, D Drudepoles exhibiting Raman-scattering and Kerr-effect, the total polarisation P_{tot} can be written as

$$\mathbf{P_{tot}} = \sum_{l=1}^{L} \mathbf{P_l} + \sum_{d=1}^{D} \mathbf{P_d} + \mathbf{P_{Kerr}} + \mathbf{P_{Raman}} \tag{1.2}$$

assuming that Ohm's law j = σE is valid. For a medium with L Lorentz-poles, D Drudepoles exhibiting Raman-scattering and

$$\nabla \wedge \mathbf{H}^{n+\frac{1}{2}} = \epsilon_0\epsilon_\infty \frac{\mathbf{E}^{n+1} - \mathbf{E}^n}{\mathbf{\Delta t}} + \frac{\mathbf{P}_{tot}^{n+1} - \mathbf{P}_{tot}^n}{\mathbf{\Delta t}} + \sigma \frac{\mathbf{E}^{n+1} + \mathbf{E}^n}{2} \tag{1.3}$$

Kerr-effect, the total polarisation P_{tot} can be written as
electric field: $\mathbf{P}_l^n = \mathbf{P}_l^n(\mathbf{E}^n)$, $\mathbf{P}_d^n = \mathbf{P}_d^n(\mathbf{E}^n)$,
$\mathbf{P}_{Raman}^n = \mathbf{P}_l^n(|\mathbf{E}^{n-1}|^2\mathbf{E}^n)$ and $\mathbf{P}_{Kerr}^n = \mathbf{P}_l^n(|\mathbf{E}^n|^2\mathbf{E}^n)$.
Apparently, all polarisations at time-step n depend linearly on the electric field E^n, except the contribution of the Kerr-effect. Ampere's law (1.1) has to be solved for E^{n+1} for which it is a cubic system of coupled equations. [1] suggest to solve this nonlinear system by using Newton's method in three dimensions to approximate the solution iteratively. This approach is quite inefficient as it requires the computation of an inverse of a 3 by 3 matrix after each iteration. Moreover, it prevents the algorithm from being parallelized. A more efficient formulation can be developed by the introduction of a new variable

$$I^n \doteq |\mathbf{E}^n|^2 \tag{1.4}$$

The resulting advantage is that all components of the system of equations (1.1) depend linearly on E^{n+1}, i.e., the system of equations is decoupled which allows to split off the different contributions from the polarisations. It remains to solve the resulting cubic update equation

$$I^{n+1} = \frac{a^2}{(b + cI^{n+1})^2} = f(I^{n+1}) \tag{1.5}$$

where the constants a, b and c are defined as follows

$$a = (\epsilon_\infty - \frac{\sigma\Delta t}{2\epsilon_0} + R^n + \alpha\chi^3 I^n)E^n + \frac{\Delta t}{\epsilon_0}\nabla \wedge H^{n+\frac{1}{2}} + \frac{1}{\epsilon_0}\Delta P$$
$$b = \epsilon_\infty + \frac{\sigma\Delta t}{2\epsilon_0} + R^{n+1}$$
$$c = \alpha\chi^3.$$

R describes the contribution from Raman- scattering and the term ΔP stands for the linear polarisation contributions by Lorentz- and Drude-poles. There are two possibilities of how to solve this equation, both have their own advantages and shall be described next. It can be shown that for positive third order susceptibilities $\chi^3 > 0$ a unique real valued solution to equation (2.3) exists, while for negative third order susceptibilities $\chi^3 < 0$ there are up to three different possible solutions from which it is hard to determine which one is correct. The solution of the positive case $\chi^3 > 0$ is given by

$$I^{n+1} = \left(-\frac{q}{2} + \sqrt{D}\right)^{\frac{1}{3}} + \left(-\frac{q}{2} - \sqrt{D}\right)^{\frac{1}{3}} - \frac{2K}{3} \tag{1.6}$$

where the constants are defined as

$$K = \frac{b}{c}$$
$$p = -\frac{K^2}{3}$$
$$q = -\left(\frac{2K^3}{27} + \frac{a^2}{c^2}\right)$$
$$D = \left(\frac{q}{2}\right)^2 + \left(\frac{p}{3}\right)^3.$$

This solution has two advantages compared with the approach of [1]:

- allows splitting up of polarisation updates contributing an additive constant to the standard update
- does not require a computationally expensive iteration

Hence, a better overall performance in speed and accuracy can be expected.

For the negative case $\chi^3 < 0$, we solve the cubic update equation (1.3) for I by performing a fixed-point iteration as the problem is bad-conditioned for other methods such as the Newton or the secant method. As it will be shown below, a criterion for the fixed-point iteration under which it converges to the correct solution can be derived analytically. The advantage of the fixed–point iteration is that it finds the correct solution regardless if the update field component lies on the material border where other field components at the same grid point have other update equations. For the analytical solution on a material border, the adjoining field update equations have to be known requiring many additional parameters to be stored in memory. Thus, it is most efficient to solve the update equation (1.3) for I on material borders and regions with negative susceptibility $\chi^3 < 0$ by applying the fixed-point iteration while at material interiors with positive third order susceptibility $\chi^3 > 0$ the analytical solution is used. This new algorithm is hence particularly efficient in voluminous materials with positive third order susceptibility $\chi^3 > 0$.

STABILITY OF THE FDTD UPDATE

In this section, the stability and phase error of our new algorithm will be derived. The used methodology is presented in [2] and [3]. As a result, a stability condition is found which determines how to chose the spatial and the temporal sampling.

The phase error of the algorithm describes how much faster or slower a numerical wave front is compared with the physical wave front. While stability depends on complex dependencies between the material parameters and the spatial and temporal grid resolution, the phase error solely depends on the spatial grid resolution and it disappears if the spatial grid resolution tends to infinity. The algorithm's accuracy also depends on the temporal resolution, i.e. on the size of the time-step because only in the limes where the time-step tends to 0, the numerical dispersion relation becomes equal to the physical dispersion relation of the simulated material. First, the numerical dispersion relation which in fact represents the phase error of the algorithm is derived. Assuming that each unknown in the system is represented as a plane wave of the form $e^{-i(\omega t - kx)}$, the temporal derivatives in the time-domain are replaced with multiplications of -iω in the frequency domain and the spatial derivative is replaced with ik. With respect to the discretized space, -iω is replaced with -iΩ and ik with iK where (in a uniform grid with = x,y,z and axis along the unit vectors ex,y,z)

$$\Omega = \frac{2}{\Delta t}\sin\left(\frac{\omega\Delta t}{2}\right)$$
$$\mathbf{K} = \frac{2}{\Delta}\left[\sin\left(\frac{k_x\Delta}{2}\right)\mathbf{e_x} + \sin\left(\frac{\mathbf{k_y\Delta}}{\mathbf{2}}\right)\mathbf{e_y} + \sin\left(\frac{\mathbf{k_z\Delta}}{\mathbf{2}}\right)\mathbf{e_z}\right]$$

Clearly, as the step size and the cell size tend to 0, the above expressions reduce to their analytical counterparts. Applying the above expressions as described to the present problem and solving the resulting system, the numerical dispersion relation for the Kerr-effect is found to be

$$\epsilon_{num} = \epsilon_\infty + \chi^3 I \tag{2.1}$$

Which is similar to the standard Yee-algorithm dispersion with an intensity dependent permittivity. Solving the numerical dispersion relation

$$\mathbf{K}\cdot\mathbf{Kc^2} = \mathbf{\Omega^2}\epsilon_{\mathbf{num}} \tag{2.2}$$

for ω in one dimension yields

$$\begin{aligned}\omega &= \frac{2}{\Delta t}\arcsin\sqrt{\frac{S^2\sin^2\left(\frac{k\Delta}{2}\right)}{\epsilon_\infty + \chi^3 I}} \\ &= \frac{2}{\Delta t}\arcsin\zeta.\end{aligned} \tag{2.3}$$

As a consequence, ω becomes imaginary if ζ > 1. Using the maximal value that ζ can reach, the following stability condition is found

$$S \leq \sqrt{\epsilon_\infty + \chi^3 I} \tag{2.4}$$

As expected, this condition depends on the field intensity and it seems that stability is increased with increasing intensity as the Courant-number S is not limited by ε but by the intensity. For low intensities, the Courant-condition of the standard FDTD algorithm applies. It is important to be aware that this condition only ensures stability of the FDTD-algorithm itself. Solving the update equation for the Kerr-effect requires to solve a non-linear equation. This has to be done either by the Newton-method used in [1] or by applying a fixed-point iteration. If these iterations converge depends on the intensity of the applied field as shown later in this section. As a consequence, the above condition does not ensure stability of the entire algorithm, but it needs to be satisfied. To determine the minimal grid sampling number N_λ, the numerical phase vector k which is given by

$$\begin{aligned}k &= \frac{2}{\Delta}\arcsin\left[\frac{\sqrt{\epsilon_\infty + \chi^3 I}}{S}\sin\left(\frac{\pi S}{N_\lambda}\right)\right] \\ &= \frac{2}{\Delta}\arcsin\xi\end{aligned} \tag{2.5}$$

has to be analysed. If ξ> 1, then k becomes imaginary which results in an aphysical exponential decay of the wave. This is the case if the grid sampling number N_λ is too small, i.e. it is required that

$$N_\lambda \geq \frac{\pi S}{\arcsin\left(\frac{S}{\epsilon_\infty + \chi^3 I}\right)} \tag{2.6}$$

As the intensity is increased, the sampling number N_λ has to be increased as well.

The verification of the simulated physics of the nonlinear algorithm is done by reproducing the qualitative behavior of the nonlinearity (e.g. soliton propagation figure 3) or by comparison with other numerical results (see figures 4 & 5). [4] suggested a very interesting approach to test the accuracy of numerical models of the third order nonlinearity: a comparison of the numerical results with the analytical solution for four-wave mixing (FWM). FWM is a process which solely depends on the third order nonlinearity and therefore the accuracy analysis is not affected by inaccuracies of dispersion models (as required for soliton simulation). FWM describes how a pump and a signal wave of frequency ω_p and ω_s respectively are converted to a frequency $\omega_c = 2\omega_p - \omega_s$ which is parametrically amplified. An output power spectrum after a pump (at 192 THz) and a signal (at 195 THz) wave traversed a slab (of length 50µm with χ^3 = 10-18) of Kerr-material is shown in figure 1. The new generated frequencies due to FWM (at 189 THz, 198 THz,...) are clearly visible.
The results of the accuracy analysis are shown in figure 2 where the signal-conversion efficiency in a nonlinear Kerr-medium as

IT'IS FOUNDATION
ETH
Eidgenössische Technische Hochschule Zürich
Swiss Federal Institute of Technology Zurich
s p e a g

a function of pump power is shown. It is found that the FDTD results asymptotically converge to the analytical solution as pump power is decreased. Generally, the FDTD method shows a smaller conversion efficiency than the analytical solution which can be explained by the fact that pump and signal depletion in the analytical formulation are ignored (an effect that grows with increasing field intensities). Moreover, the so-called small-signal condition used in the analytical derivation is not valid anymore for strong beam intensities. Overall, high accuracy for the new FDTD formulation of the third order susceptibility can be assessed.

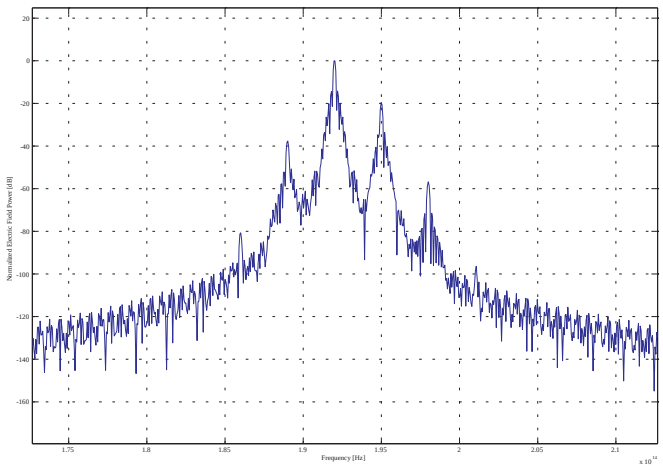

Figure 1: Electric field power spectrum after pump (at 192 THz) and signal (at 195 THz) wave traversed a slab (of length 50m with $\chi = 10^{-18}$) of Kerr-material. The new generated frequencies due to FWM (at 189 THz, 198 THz,...) are clearly visible

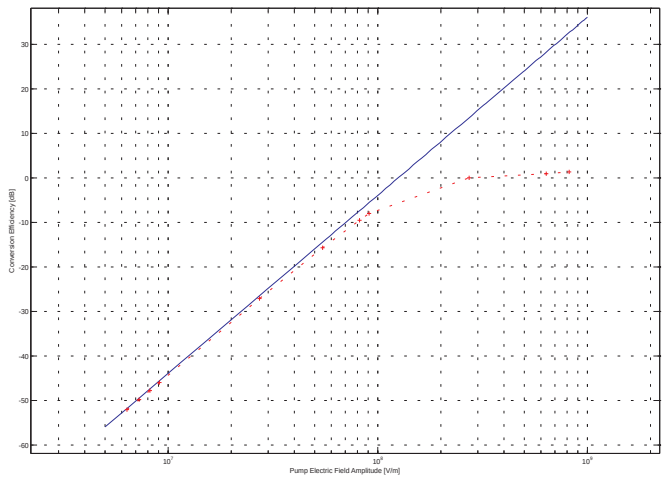

Figure 2: Signal-conversion efficiency in a nonlinear Kerr-medium as a function of pump power. The solid line is the analytical solution, the dotted line results from our new FDTD scheme. For high pump powers, pump and signal depletion is observed giving rise to a strong deviation from the analytical solution.

CONVERGENCE OF THE FIXED-POINT ITERATION

The convergence of the fixed point iteration which is needed to solve for the Kerr-effect is proven by using Banach's fixed point theorem. For simplicity, the third-order susceptibility χ^3 shall be written without the susceptibility index, i.e., $\chi = \chi^3$, for the rest of this section. Banach's fixed point theorem is applied to $f(I^{n+1})$ which has been defined in equation (1.5). To this end, it has first to be shown that the first derivative of $f(I^{n+1})$ is limited for all I^{n+1} at least within an interval D:

$$f'(I^{n+1}) = \frac{-2a^2c}{(b + cI^{n+1})^3} \tag{3.1}$$

Apparently, the supremum of $|f'(I^{n+1})|$ is found where $I^{n+1} = 0$ and is given by

$$S = \sup_{I^{n+1} \in D} |f'(I^{n+1})| = \frac{2a^2c}{b^3} \tag{3.2}$$

Next, it has to be shown that the above supremum S is smaller than 1 such that $f(I^{n+1})$ is Lipschitz-continuous with a Lipschitz-constant $L \leq 1$ and consequently, $f(I^{n+1})$ is a contraction on the interval D and the fixedpoint iteration will be convergent on D. The condition for $f(I^{n+1})$ to be a contraction on D can be written as

$$a^2c \leq \frac{b^3}{2} \tag{3.3}$$

As long as this condition holds the fixed-point iteration will converge. Thus, using a smaller Courant-number increases the value of maximal intensity for which the fixed-point iteration converges (as the term proportional to H becomes smaller). It is possible to derive a simple expression for the maximal possible intensity $I = |E|^2$ for which the fixed-point iteration still converges. To this end, the two extremal cases for the Kerr-effect are considered:

1. no Kerr-effect, only Raman-scattering is present c = 0 and equation (3.3) is always satisfied (but the fixed point iteration would not be required)

2. only Kerr-effect is present, no Raman-scattering $R^n = 0$

For the second case, the inequality (3.3) has to be further analysed. Apparently, the inequality (3.3) will be strengthened by the presence of a positive conductivity (for negative conductivities, one can argue that the entire term is small as the timestep is small). Thus, in order to further reduce the complexity, set $\sigma = 0$. Due to the nature of continuity of the used equations, respectively because the temporaland spatial grid have accurately high resolutions, the terms containing spatial and temporal derivations can be considered small compared with the term proportional to the electric field and can hence be neglected. Thus, the contraction condition can now be written as

$$[(\epsilon_\infty + \chi I^n)E^n]^2 \chi \leq \frac{\epsilon_\infty^3}{2} \tag{3.4}$$

By introducing the characteristic Convergence-Intensity

$$C = \frac{\epsilon_\infty}{\chi} \tag{3.5}$$

equation (3.3) can be rewritten as

$$I^3 + 2CI^2 + C^2I - \frac{C^3}{2} \leq 0 \tag{3.6}$$

This is a simple cubic equation which can be solved analytically. It can be shown that it has only one real valued solution which defines the maximal intensity for which the fixed-point iteration still converges:

$$I_{max} = 0.96|C| \tag{3.7}$$

Thus, also the electric field amplitude E^n is limited to an upper value. The convergence intervall is $[0, I_{max}]$. Furthermore, one has to be aware that the above result is an upper limit which lies too high because some terms were neglected. As a consequence, it is recommended to choose amplitudes that are enough below the above limit. In this context it is interesting to note, that also the Newton-iteration used by [1] becomes unstable for field amplitudes resulting in similar values as I_{max}.

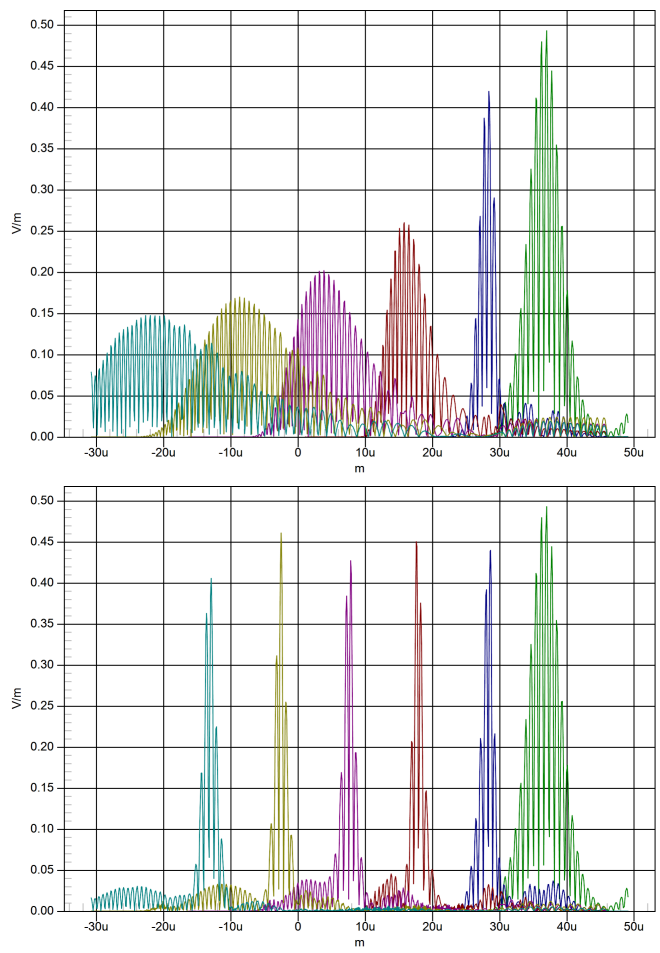

Figure 3: 1D-simultaion: A secant-pulse is launched (green) and enters a linear dispersive Lorentz-medium (upper) and a nonlinear dispersive Lorentz-medium with Kerr-effect and Raman-scattering (lower) at 30 µm. The electric field amplitude is shown at different times. The linear dispersion gives rise to pulse-broadening. In the non-linear medium, a soliton is formed which propagates whithout changing its shape and the formation of a precursor pulse is observed.

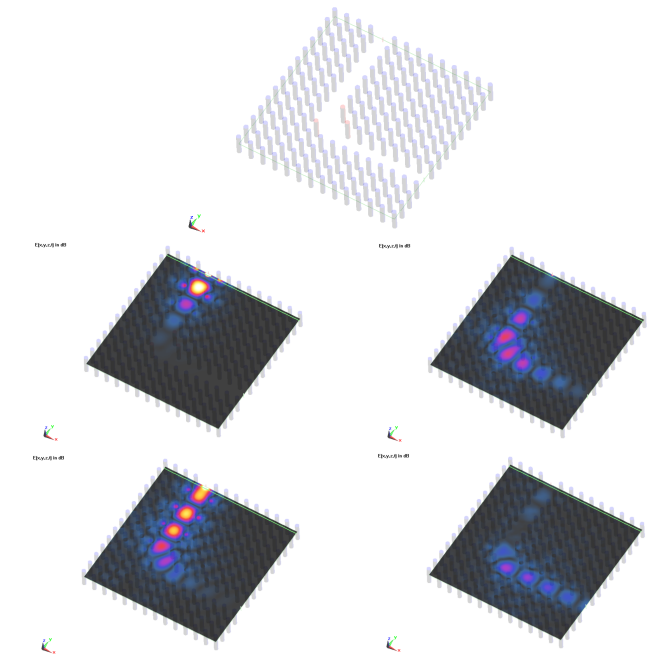

Figure 4: A Gaussian-pulse is launched into a photonic crystal waveguide consisting of dielectric rods. Placing 3 nonlinear rods at the waveguide bend (marked red) improves its transmitance for most frequencies (see figure 5).

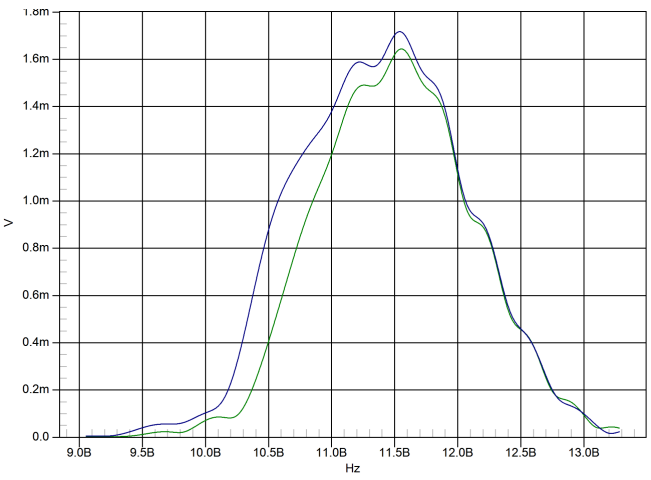

Figure 5: Power-spectrum of the transmitted pulse at the waveguide exit of figure 4. The nonlinear photonic crystal has increased transmittance (blue) for lower frequencies.

CONCLUSIONS

A novel algorithm that tremendously increases the efficiency of the FDTD method applied to materials with third-order nonlinear susceptibility has been developed and applied to various benchmarks. The core advantage of the approach being that it allows parallelisation of the algorithm and its computational efficiency, particularly for materials with positive third order susceptibility. The three dimensional algorithm was successfully implemented into the fully featured FDTD EM platform SEMCAD X.

Physical accuracy has been investigated by simulating FWM assessing high accuracy for low intensities. For intensities sufficiently lower than the characteristic Convergence-Intensity (3.5) it has been shown analytically that the applied fixed-point iteration converges to the correct value. Furthermore, the stability analysis of the new FDTD scheme revealed that the algorithm is stable under the Courant-stability condition of the standard FDTD scheme.

The performed benchmarks such as soliton simulation and the simulation of a nonlinear PC showed excellent agreement between the findings of other nonlinear FDTD schemes and the one presented here.

REFERENCES

[1] *J. H. Greene and A. Taflove. General Vector Auxiliary Differential Equation Finite-Difference Time-Domain Method for Nonlinear Optics. Optics Express, 14:8305–8310, 2006.*

[2] *A. Taflove and S. C. Hagness. Computational Electrodynamics, The Finite-Difference Time-Domain Method. Artech House, 2005.*

[3] *J. L. Young. Propagtion in Linear Dispersive Media: Finite Difference Time-Domain Methodologies. IEEE Transactions on Antennas and Propagation, 43:422–426, 1995.*

[4] *M.Fuji et al. A Simple and Rigorous Verification Technique for Nonlinear FDTD Algorithms by Optical Parametric Four-Wave Mixing. Microwave and Optical Technology Letters, 48:88–91, 2006.*